TRANSONIC FILM-COOLING INVESTIGATIONS: EFFECTS OF HOLE SHAPES AND ORIENTATIONS

S. Wittig, A. Schulz, M. Gritsch, and K.A. Thole*
Lehrstuhl und Institut für Thermische Strömungsmaschinen
Universität Karlsruhe (T.H.)
76128 Karlsruhe, Germany

ABSTRACT

The emphasis of the present study is to understand the effects of various flowfield and geometrical parameters in the nearfield region of a scaled-up film-cooling hole on a flat test plate. The effect of these different parameters on adiabatic wall effectivenesses, heat transfer coefficients, discharge coefficients and the near-hole velocity field will be addressed. The geometrical parameters of concern include several angles of inclination and rotation of a cylindrical film-cooling hole and two different hole shapes - a fanshaped hole and a laidback fanshaped hole. The fluid dynamic parameters include both the internal and external Mach number as well as the mainstream-to-coolant ratios of total temperature, velocity, mass flux, and momentum flux. In particular, the interaction of a film-cooling jet being injected into a transonic mainstream will be studied.

This paper includes a detailed description of the test rig design as well as the measuring techniques. Firstly, tests revealing the operability of the test rig will be discussed. Finally, an outlook of the comprehensive experimental and numerical program will be given.

NOMENCLATURE

C_D	Discharge coefficient
D	Film-cooling hole diameter
H_{12}	Ratio of boundary layer displacement thickness δ_1 to momentum thickness δ_2
I	Jet-to-crossflow momentum ratio
L	Film-cooling hole length measured along the centerline axis
M	Blowing ratio
Ma	Mach number
$\dot{m}$	Mass flow rate
p	Static pressure
p_t	Total pressure
Re_D	Reynolds number based on film-cooling hole diameter
T_t	Total temperature
u,v	Streamwise and vertical components of the mean velocity vector
x	Streamwise distance from hole centerline
y	Vertical distance from main channel wall
Greek	
α	Angle of inclination
γ	Angle of rotation
δ_{99}	Boundary layer thickness, 99 % point
Subscripts	
c	Internal flow conditions
m	External flow conditions
AW	Adiabatic wall conditions

INTRODUCTION

Increasing turbine inlet temperatures require an effective cooling of turbine vanes and blades. Modern airfoils are equipped with a complex cooling regime combining various

*Present Address: Mechanical Engineering Department
University of Wisconsin
1513 University Avenue
Madison, Wisconsin 53706-1572

Presented at the International Gas Turbine and Aeroengine Congress & Exhibition
Birmingham, UK — June 10-13, 1996

convection cooling methods on the inner surface and film-cooling on the outer surface. Primarily film-cooling still offers a big potential for improvements and is, therefore, the subject of numerous research activities.

The injection of discrete film-cooling jets into a two dimensional boundary layer induces a complicated three-dimensional flowfield which depends on many geometrical and fluid dynamic parameters. As a direct consequence, the heat transfer is also dictated by the same parameters.

The present study focuses on the detailed investigation of the throughflow characteristics of film-cooling holes and on the determination of the nearfield heat transfer and film-cooling effectiveness. To get a detailed insight into the flow structure, the investigations are performed on a scaled-up single hole ejection configuration. The test rig is carefully designed to meet realistic film cooling parameters. According to various locations of film-cooling holes on a real airfoil with different orientations of the holes, both with respect to the external flow as well as with respect to the internal coolant passage flow, the test rig permits an independent rotation of the coolant supply channel and the film-cooling hole itself. Moreover, different hole geometries, e.g. cylindrical holes, fanshaped holes, and laidback fanshaped holes, can be tested by replacing the junction between the two channels. Mach numbers up to 1.2 in the external flow channel and up to 0.6 in the internal flow channel can be achieved.

Few studies have investigated the influence of contoured film-cooling holes. In most cases, the holes are cylindrical with a diffuser shaped expansion at the exit portion of the hole. Goldstein, Eckert, and Burggraf (1974) examined holes with lateral expansion of 10° at the hole exit portion, while Makki and Jakubowski (1986) tested holes with a trapezoidal cross-sectional area at the exit. The increased cross-sectional area at the hole exit compared to a standard cylindrical hole leads to a reduction of the mean velocity and, thus, of the momentum flux of the jet exiting the hole. Therefore, the penetration of the jet into the main flow is reduced resulting in an increased cooling efficiency. Furthermore, lateral expansion of the hole provides an improved lateral spreading of the jet leading to a better coverage of the airfoil in spanwise direction and a higher spanwise averaged film-cooling efficiency. Hay and Lampard (1995) investigated cylindrical holes with a lateral expansion angle of 12.5° (flared holes) and holes with an additional layback of 7.5°. It was found that the discharge coefficient of flared holes is higher than for cylindrical holes. The layback does not further increase the discharge coefficient. Haller and Camus (1983) performed aerodynamic loss measurements on a 2D transonic cascade. Holes with a spanwise flare angle of 25° were found to offer significant improvements in film-cooling effectiveness without any additional loss penalty.

The improved spreading of the jet and a delayed separation at high momentum ratios are the reasons why film-cooling holes with compound angle orientations have gained attention in the literature (e.g. Schmidt, Sen, and Bogard (1994), Ligrani, Wigle, Ciriello, and Jackson (1994), Honami, Shizawa, and Uchiyama (1992), Sathyamurthy and Patankar (1990), Jubran and Brown (1985), Colladay and Russell (1976) and Goldstein, Eckert, Eriksen, and Ramsey (1970)). These holes are found to provide a significantly improved thermal protection of the blade surface compared to streamwise injection, in particular at elevated momentum ratios. On the other hand, Sen, Schmidt, and Bogard (1994) reported increased heat transfer rates due to an enhanced interaction between the jet and the main flow, particularly at high momentum ratios .

The numerical studies of Leylek and Zerkle (1993), Garg and Gaugler (1995) and Benz, Wittig, Beeck, and Fottner (1993) address the effect of the flow inside the cooling hole influencing the overall film-cooling flowfield. Since the flowfield inside the hole is strongly affected by the way the coolant is supplied to the film-cooling hole, a plenum chamber, widely used for experimental studies, is not a correct means to represent the internal coolant passage flow of an airfoil. The effect of the coolant supply channel compared to a plenum on the flow inside the film-cooling hole will be discussed in detail by Thole, Gritsch, Schulz, and Wittig (1996a).

Liess (1975) studied the effect of the main flow Mach number on the film-cooling parameters. Mach numbers up to 0.9 were employed. No measurable effect on film-cooling efficiency was found, when the main flow recovery temperature is used as reference temperature. However, no studies are present in the literature examining the effect of transonic main flow Mach numbers for discrete hole film-cooling in the near-hole region.

TEST RIG DESIGN

When designing the test rig, the major intention was to simulate as many geometrical and flow parameters of a real airfoil as possible. As a result of comprehensive analyses it was found that it is possible to match the Mach and Reynolds numbers of the coolant as well as of the main flow. Furthermore, realistic coolant-to-mainflow temperature ratios, pressure ratios, blowing ratios, momentum ratios and boundary layer thickness to hole diameter ratios can be achieved. In choosing the facility and in designing the experiment, the test conditions given in Table 1 were considered.

Calculations were done to determine the possible experimental regimes. By minimizing the total pressure of the mainstream, the maximum possible cross-sectional area can

Hole Diameter	D	10 mm
Internal pressure	p_{tc}	up to 2 Bars
Internal temperature	T_{tc}	290 K
Pressure ratio	p_{tc}/p_m	1 ...2
Temperature ratio	T_{tc}/T_{tm}	1 ...2
Internal Mach number	Ma_c	0 ...0.6
External Mach number	Ma_m	0 ...1.2
Internal Reynolds number	Re_{Dc}	up to $2.5*10^5$
External Reynolds number	Re_{Dm}	up to $2.1*10^5$
Boundary layer thickness	δ_{99}/D	0.5

TAB. 1: Operational conditions of the film-cooling test rig

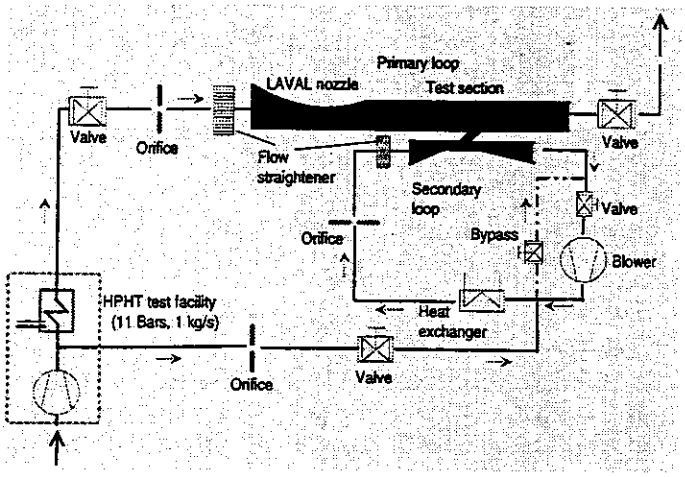

FIG. 1: Film-cooling test rig

be achieved for a given mainstream flow rate. Maximizing the cross-sectional area is desirable to ensure that there is no side or top wall interference on the film-cooling flowfield. As a consequence, the static pressure in the test section is far below ambient pressure for the transonic flow case.

EXPERIMENTAL APPARATUS

The present investigation was carried out in a continous flow wind tunnel at the Institut für Thermische Strömungsmaschinen (ITS), Karlsruhe (see Fig. 1). The air was supplied by a high pressure, high temperature (HPHT) test facility. The facility is able to provide a maximum flow rate of 1 kg/s at a maximum temperature and pressure of 1120 K and 11 Bars, respectively.

The film-cooling test section consists of a primary loop representing the external flow and a secondary loop representing the internal flow (see Fig. 2).

Primary Loop

The air supplied by the HPHT test facility passes a metering orifice and flow straighteners before entering the test

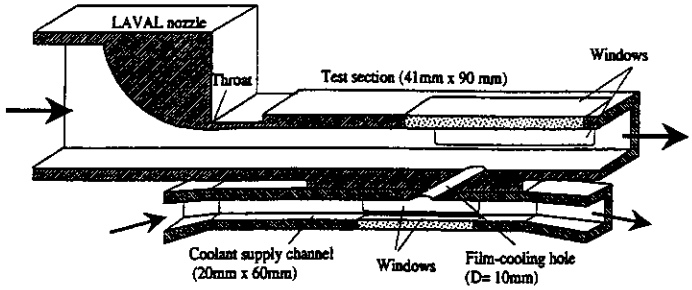

FIG. 2: Film-cooling test section

section through a LAVAL nozzle. This nozzle was specifically designed based on a method of characteristics solution for Ma_m=1.2.

The test section is 90 mm in width and 41 mm in height. For transonic flow conditions the height is reduced to 32 mm. Using an adjustable upper wall, a zero pressure gradient in streamwise direction is set in the test section. The test section side walls and the top wall have quartz glass windows to enable good optical access allowing Schlieren and Laser Doppler Velocity (LDV) measurements. The quartz glass window in the top wall can be replaced by a sapphire window required for surface temperature measurements using a infrared (IR) camera system.

Secondary Loop

An accurate measurement of the flow rate through the film-cooling hole is indispensable for an exact determination of the flow parameters, in particular the discharge coefficient. The standard configuration for measuring the flow rate for the case of crossflow on both, entry and exit side of the hole, is the "open" loop (Fig. 3(a)). The flow rates in the coolant supply channel are measured up- and downstream of the film-cooling hole location using orifices A and B. The difference between these two flow rates is equal to the flow rate through the hole. For the case when the flow rate through the hole is only a few percent of the flow rate in the coolant supply channel the uncertainty of the calculated flow rate through the hole is of the same magnitude as the flow rate through the hole itself. Thus, this configuration can not be used to get accurate measurements of the flow rate through the hole.

For this reason, the secondary loop used for the present study is a recirculating channel ("closed" loop) with only one inlet, which is supplied by the compressor, and one exit, which is exhausted through the film-cooling hole (Fig. 3(b)). With this configuration the flow rate through the film-cooling hole is obtained directly, independently of the crossflow flow rate. The flow rate entering the secondary loop which is equal to the flow rate leaving the secondary loop through the film-cooling hole, is measured using orifice C.

The secondary loop itself acts like a plenum.

The orientation of the coolant supply channel with respect to the main channel can be set within 0° (parallel flow) to 90° (perpendicular flow) and 180° (counter parallel flow) to account for the various flow configurations in cooled airfoils in relation to film-cooling holes discussed in Hay, Lampard, and Benmansour (1983).

The major components of the secondary loop include a blower, a heat exchanger and a flow section where flow is ejected through the film-cooling hole into the mainstream. Flow for the secondary loop is provided by the HPHT test facility as well. However, the total pressure in the secondary loop can be set independently from the primary loop. The flow in the secondary loop is driven by an additional blower. Thus, the Mach number can be set by adjusting the volume flow rate circulating in the secondary loop using a throttling valve upstream of the blower and a bypass line parallel to the secondary loop. The majority of the secondary loop has a large pipe diameter of 125 mm, to reduce the pressure losses, while the cross-sectional area at the film-cooling hole is 60 mm in width and 20 mm in height.

The blower continually supplies energy to the flow circulating in the secondary loop resulting in a continous increase of the temperature of the flow. Therefore, a water-cooled heat exchanger is introduced to the secondary loop downstream of the blower. The temperature of the circulating flow can be controlled by adjusting the amount of coolant water going through the heat exchanger.

Film-cooling Hole Geometries

All tests were carried out using single scaled-up film-cooling holes. In total, seven hole geometries (five cylindrical holes and two shaped holes) were tested (see Table 2). The hole geometries were decided in cooperation with the industrial partners involved in the present research program.

The diameter of the cylindrical holes and the diameter of the cylindrical inlet section of the shaped holes were 10 mm. The thickness of the wall was 30 mm and kept constant for all hole geometries.

The lateral expansion angle of both shaped holes was 14°, resulting in a hole width of 30 mm at the hole exit. The forward expansion angle of the laidback fanshaped hole was 15°, resulting in a hole length of 40 mm at the hole exit. A sketch of the 30° inclined cylindrical and both shaped holes is given in Fig. 4.

INSTRUMENTATION AND MEASURING TECHNIQUES

The quantities of interest comprise adiabatic wall effectivenesses, heat transfer coefficients, discharge coefficients,

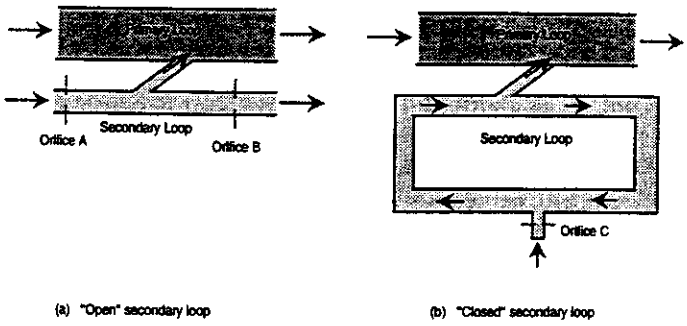

FIG. 3: Configurations for measuring the mass flow rate through the film-cooling hole

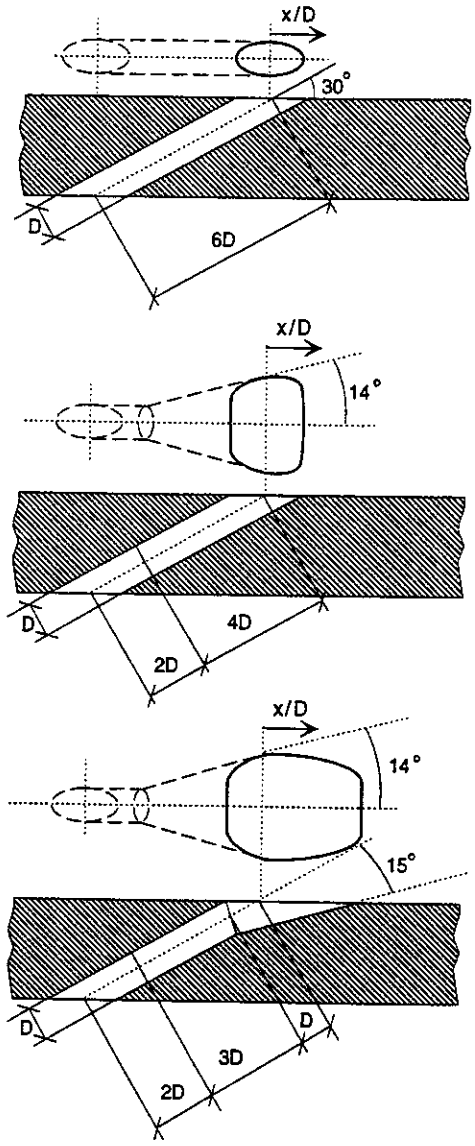

FIG. 4: Cylindrical, fanshaped, and laidback fanshaped hole geometries

	Hole geometry	Hole diameter D [mm]	Angle of inclination α	Angle of rotation γ	Hole length-to-diameter ratio L/D
1	cylindrical	10	30°	0°	6
2	cylindrical	10	45°	0°	4.24
3	cylindrical	10	90°	0°	3
4	cylindrical	10	30°	45°	6
5	cylindrical	10	30°	90°	6
6	fanshaped	10	30°	0°	6
7	laidback fanshaped	10	30°	0°	6

TAB. 2: Film-cooling hole geometries

and a map of the flowfield in the vicinity of the ejection hole. Three different types of test plates have been designed including one for adiabatic effectiveness measurements, one for heat transfer coefficient measurements, and one for discharge coefficient measurements and flowfield mapping. The test plates are equipped with removable inserts which allow for different cooling hole geometries and cooling hole orientations relative to the external flow.

Adiabatic Wall Effectiveness Test Plate

Finite element analyses were performed to select a proper material for achieving an adiabatic boundary condition. Several materials were evaluated in terms of enduring a nominal temperature of 600 K to enable a coolant-to mainstream temperature ratio of about 2 and having a low thermal conductivity to minimize errors due to heat conduction. The computations indicated that a high temperature plastic (TECAPEK) with a thermal conductivity of 0.2 W/mK and a maximum operating temperature of about 580 K meets those requirements. Surface temperatures are measured using both thermocouples placed on the surface of the test plate and an AGEMA 870 IR camera system (Fig. 5). Sixteen Ni-NiCr thermocouples were located from 0.5 D to 10 D downstream of the hole trailing edge on the hole centerline. Fourteen Ni-NiCr thermocouples are positioned at streamwise locations of 1 D, 3 D and 6 D at a lateral distance of -3.5 D to 4 D from the hole centerline.

The IR camera system provides a two dimensional distribution of the temperature on the plate surface. The image of the test plate surface is digitized into an array of 140x140 pixels. Accounting for the optical setup used with the IR camera a spatial resolution of about 1 mm^2 per pixel could be achieved. Actually, a calibration of the system is not necessary, because the test plate surface is covered by black paint of a well-known emissivity of 0.95. However, there are some parameters influencing the measurements which are difficult to quantify. Therefore, some of the thermocouples mentioned above are used for re-calibrating the IR camera system to increase the accuracy of the temperature measurements. Details of surface temperature measurements

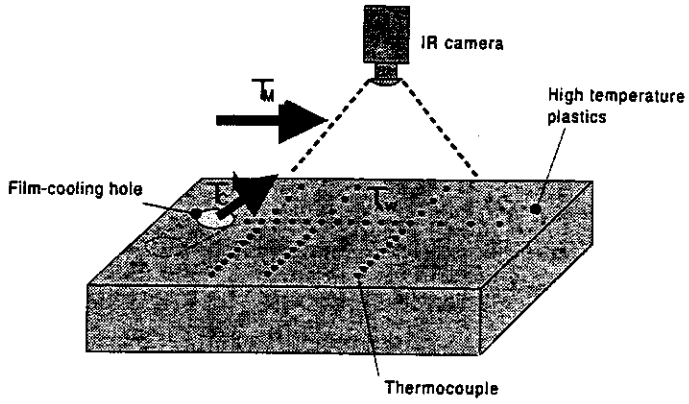

FIG. 5: Adiabatic wall effectiveness test plate

using the IR camera system are given by Scherer, Wittig, Morad, and Mikhael (1991) and Martiny, Schulz, and Wittig (1995).

Heat Transfer Test Plate

Finite element analyses were also used for designing the heat transfer test plate. It is a dual layer test plate with a TECAPEK layer on top of a copper block. The optimum thickness of this plastic layer was calculated to be 3.5 mm resulting in a minimum uncertainty of the heat transfer coefficient. The copper block is maintained at a constant temperature by internal water cooling (Fig. 6). The surface temperature is measured with the IR camera. Additionally, seven Ni-NiCr thermocouples are distributed on the plate surface used for re-calibrating the IR camera.

The surface temperature of the test plate and the temperature of the copper block are used as boundary conditions for a finite element analysis. In calculating the heat flux perpendicular to the surface of the test plate the heat transfer coefficient can be determined.

Discharge Test Plates

For investigating the discharge coefficients seven test plates (one for each hole geometry) were manufactured. The

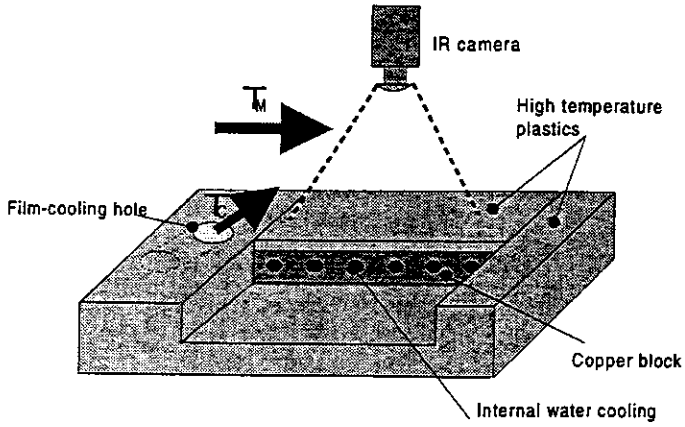

FIG. 6: Heat transfer test plate

test plates were made of aluminium allowing a very accurate machining of the hole. Errors in determining the hole size and, thus, in calculating the discharge coefficient were therefore very small. The plates were also used for performing the flowfield measurements.

EXPERIMENTAL AND NUMERICAL PROGRAM

Discharge coefficient measurements: Each hole geometry was tested for a matrix of three internal Mach numbers (Ma_c=0.0, 0.3, 0.6) and four external Mach numbers (Ma_m=0.0, 0.3, 0.6, 1.2) over a range of pressure ratio p_{tc}/p_m of 1 to 2. Moreover, each hole geometry was tested at four pressure ratios (p_{tc}/p_m=1.1, 1.25, 1.4, 1.6) over a range of internal Mach number Ma_c=0.0 to 0.6 for a constant external Mach number Ma_m of 0.0. Primary and secondary loop were positioned either parallel or perpendicular to each other.

Adiabatic wall efficiency and heat transfer measurements: Each hole geometry was tested for a matrix of three internal Mach numbers (Ma_c=0.0, 0.3, 0.6) and three external Mach numbers (Ma_m=0.3, 0.6, 1.2) over a range of blowing ratio M=0.25 to 2. Primary and secondary loop were positioned either parallel or perpendicular to each other.

Flowfield visualization using Schlieren: Schlieren flow visualization were performed for the transonic flow cases to get an impression of the overall near-hole flowfield. In particular, the shock pattern of the jet/main flow interaction was addressed.

Flowfield measurements using a LDV: Three hole geometries, comprising the baseline 30° inclined cylindrical hole, the fanshaped hole, and the laidback fanshaped hole, were tested under isothermal flow conditions. Both the blowing ratio and the momentum ratio were of unity. Two main flow mach numbers were chosen (0.25 and 1.2). The coolant Mach number was kept constant at 0.3. Mean velocity components and turbulence quantities were obtained at the hole inlet, inside the hole, at the hole exit as well as in the primary channel upstream and downstream of the film-cooling hole. The primary and secondary loop were positioned parallel to each other.

Numerical flowfield and heat transfer computations: The numerical study was performed using a three-dimensional, elliptic Navier-Stokes code. For turbulence closure, the standard k-ϵ model with wall functions was applied. The governing equations were formulated in a body-fitted, non-orthogonal, curvilinear coordinate system. The code was based on a fully conservative, structured, finite volume discretization method. The transport equations were solved using a non-staggered grid. In order to subdivide the complex computational domain into simple blocks, a multiblock technique was used. The coupling of the blocks was achieved by applying periodic boundary conditions (Benz and Wittig 1992).

The SIMPLE algorithm of Patankar and Spalding (1972) was used for coupling the velocity and pressure field. This pressure-correction method was extended in order to predict transonic and supersonic flows up to Ma=3. For the discretization of the diffusive terms, a second order, central difference scheme was used, whereas the convective terms of all transport equations were discretisized by the second order accurate Monotonized-Linear-Upwind (MLU) scheme (Noll 1992). The system of algebraic equations was solved using a generalized conjugate gradient iterative procedure in conjunction with an incomplete lower-upper decomposition (ILU-CG) (Noll and Wittig 1991). The ILU-CG method was tested for a variety of computations of complex gas turbine flows and was found to be very fast and robust.

The capabilities and performance of the code were demonstrated for gas turbine flow applications by Benz, Wittig, Beeck, and Fottner (1993), Kurreck and Wittig (1994), and Wittig, Bauer, and Noll (1987). Due to the insufficient resolution of the near wall region the standard k-ϵ with wall functions approach was not suitable for heat transfer predictions. Therefore, low-Reynolds number k-ϵ turbulence models were implemented into the code (Giebert, Bauer, and Wittig 1996).

PRELIMINARY TESTING

The most important thing in the beginning was to make sure that the flow rate entering the secondary loop, which is measured by a calibrated orifice, is equal to the flow rate exiting the loop through the film-cooling hole. Therefore, comprehensive leakage tests were performed. The test plate with the film-cooling hole was replaced by a impermeable

test plate. After pressurizing the secondary loop the valve at the secondary loop inlet was closed. The pressure decay inside the secondary loop was monitored. From this information, the leackage flow rate could be derived. It was found that the leakage flow rate was about 10 % of the ideal flow rate through the film-cooling hole, assuming an isentropic expansion from the pressure inside the loop to ambient pressure. Most of the leakage flow occured at the shaft packing of the blower introduced in the secondary loop. By applying a proper counterpressure at the shaft packing the leakage flow rate was reduced to much less than 1 % of the ideal flow rate through the film-cooling hole.

Wall boundary layer profiles were taken 5 D upstream of the film-cooling hole in the main channel indicating that the naturally developing boundary layer is fully turbulent. For the low speed case (Ma_m=0.3), δ_{99}/D was 0.6 and H_{12} was 1.38. The freestream turbulence level was measured to be 1.4 %. For the high speed case (Ma_m=1.2) δ_{99}/D was 0.4 and H_{12} was 1.42. The freestream turbulence level in this case was 2.3 %. The boundary layer in the coolant supply channel 7 D upstream of the film-cooling hole entry was also found to be turbulent. The freestream turbulence level there was 1 %.

At several axial positions in both the main and the coolant supply channel, velocity profiles in lateral direction were taken to check the spanwise uniformity of the main flow, the coolant supply flow, and the flow through the film-cooling hole itself.

RESULTS

This section provides examples of the results achieved within the present study.

Discharge Coefficients

The discharge coefficient C_D is the ratio of the actual mass flow rate to the ideal mass flow rate through the film-cooling hole. The ideal mass flow rate is calculated assuming an isentropic one-dimensional expansion from the total pressure in the secondary loop p_{tc} to the static pressure in the primary loop p_m.

Figure 7 shows a typical result for the cylindrical hole (α=30°,γ=0°). The discharge coefficient is plotted versus the pressure ratio across the hole at four different Mach numbers in the primary loop (Ma_m=0.0, 0.3, 0.6, and 1.2) and a Mach number Ma_c of 0.3 in the secondary loop.

The effect of Ma_m is to reduce the discharge coefficient, particularly at low pressure ratios. This effect is more pronounced at high Mach numbers Ma_m in the primary loop. At high pressure ratios a plateau value of 0.87 for the discharge coefficient was found, independent of the Mach number Ma_m applied. Additionally, results of Hay, Lampard,

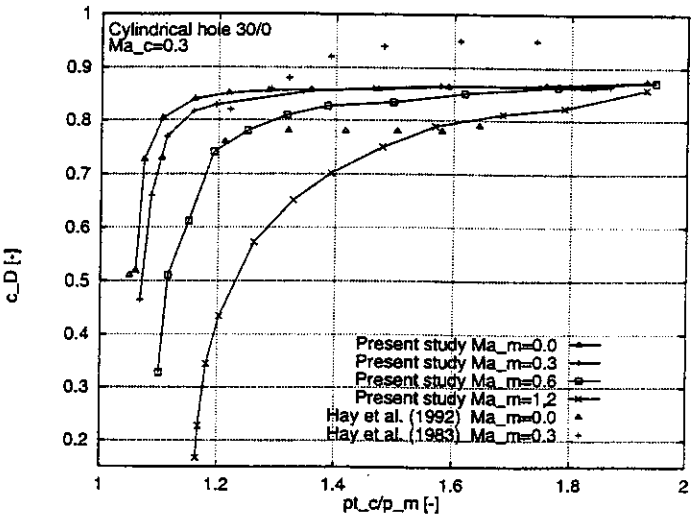

FIG. 7: Discharge coefficient C_D plotted versus pressure ratio p_{tc}/p_m for Ma_c=0.3 for the cylindrical hole (α=30°,γ=0°)

and Benmansour (1983) and Hay, Henshall, and Manning (1992) are plotted in Fig. 7. The inclination angle of the hole and the hole length-to-diameter ratio are the same as in the present study. However, it was found that for the case of Ma_m=0.0 the discharge coefficients of the present study are up to 10% higher whereas for the case of Ma_m=0.3 the discharge coefficients are up to 10% lower than reported by Hay and co-workers. Unlike the present study, they do not show a common plateau value existing at high pressure ratios.

Adiabatic Wall Effectiveness

Centerline measurements of the adiabatic wall effectiveness η of the basecase cylindrical hole (α=30°,γ=0°) at M=0.61 and I=0.22 up to 10 D downstream of the hole are presented in Fig. 8. The origin of the streamwise coordinate, x/D=0, is located at the trailing edge of the hole for the present plot. Published data of Sinha, Bogard, and Crawford (1990) and Schmidt, Sen, and Bogard (1994) are used for validating the present results since the flow parameters as well as the hole geometry are similar to the present study. Excellent agreement between the present results and the data of Schmidt, Sen, and Bogard (1994) was found. The deviations occuring from the data of Sinha, Bogard, and Crawford (1990) are believed to be due to the different hole length-to-diameter ratio, L/D=6 for the present study compared to L/D=1.75 of Sinha, Bogard, and Crawford (1990). The flow entering an orifice is known to form a vena contracta within an orifice and to re-attach about 2 D downstream of the orifice inlet (Hay and Spencer 1991). For very short film-cooling holes such as used by Sinha, Bogard,

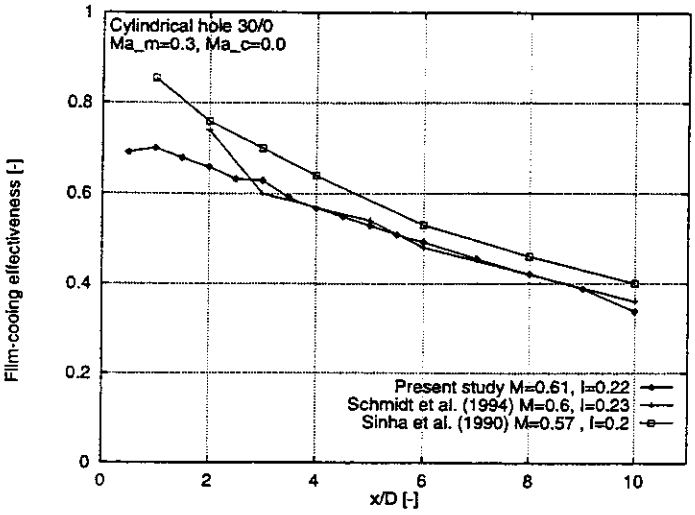

FIG. 8: Centerline film-cooling effectiveness of the cylindrical hole (α=30°,γ=0°) at Ma_m=0.3 and Ma_c=0.0

and Crawford (1990), the jet leaves the hole as a divergent streamtube and, thus, stays closer to the wall resulting in elevated film-cooling effectiveness in the vicinity of the hole.

Flowfield Visualization using Schlieren

Before comprehensive flowfield studies were performed Schlieren were used to get a qualitative impression of the near-hole flowfield in the case of transonic flow conditions. Figure 9 shows the near-hole flowfield in the primary channel for the laidback fan shaped hole. The Mach number Ma_m of the flow in the primary channel was 1.2 and the Mach number Ma_c of the flow in the secondary channel was 0.3. The blowing ratio and the momentum ratio were of unity.

It was observed that the injected coolant acts as an obstacle to the flow in the primary loop resulting in a strong shock wave immediately upstream of film-cooling hole. Downstream of the hole a weak recompression shock wave could be detected. The position and the shape of these shock waves were found to be strongly dependent on both the hole shape and the blowing rate.

Flowfield Measurements

Mean velocity vector profiles at 13 x/D-locations in the primary channel for the basecase cylindrical film-cooling hole ejection (α=30°,γ=0°) are shown in Fig. 10. The upstream and downstream edges of the hole are indicated by the lines placed on the x-axis. The Mach number Ma_m of the flow in the primary channel was 1.2 and the Mach number Ma_c of the flow in the secondary channel was 0.3. The blowing ratio and the momentum ratio were of unity. Although the blowing ratio and the momentum ratio were

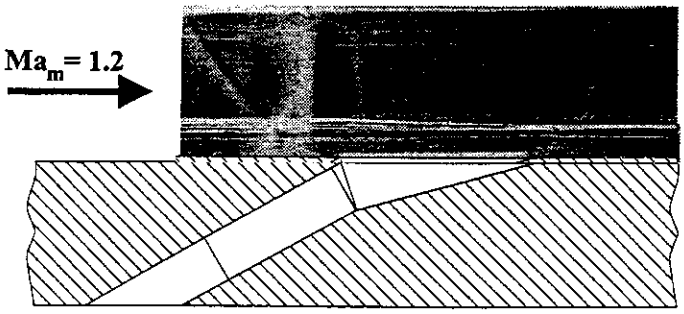

FIG. 9: Flowfield visualization using Schlieren

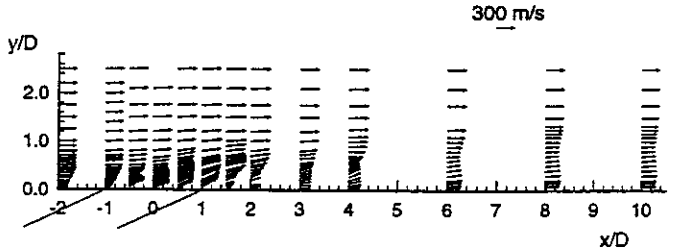

FIG. 10: Measured velocity vectors on centerline plane of the primary channel (Ma_m=1.2, Ma_c=0.3, M=1, I=1) for the basecase cylindrical hole ejection (α=30°,γ=0°)

kept constant, the velocity distribution of the jet at the hole exit was found to be more uniform compared to the low Mach number case. Measurements inside the hole and in the hole exit plane as well as numerical computations revealed that the elevated pressure ratio, which is necessary to apply a blowing ratio M=1 for the high Mach number case, causes an altered flowfield inside the hole resulting in higher vertical velocities at the upstream portion of the hole exit.

Detailed results of the flowfield measurement performed for the low Mach number case (Ma_m=0.25) are reported by Thole, Gritsch, Schulz, and Wittig (1996b).

Numerical Flowfield Computations

Numerical simulations were performed for the cylindrical, fanshaped, and laidback fanshaped hole geometries at both subsonic and transonic primary flow conditions. In the results presented below, only the subsonic flow case for the cylindrical hole will be considered.

The computational grid was generated using the multiblock technique. It consists of three blocks (primary channel 135 000 grid points, cooling hole 10 000 grid points and secondary channel 33 000 grid points). CPU time was about 90 min on a Siemens Nixdorf SNI 600/20 vector computer.

As boundary conditions, the total pressure and total tem-

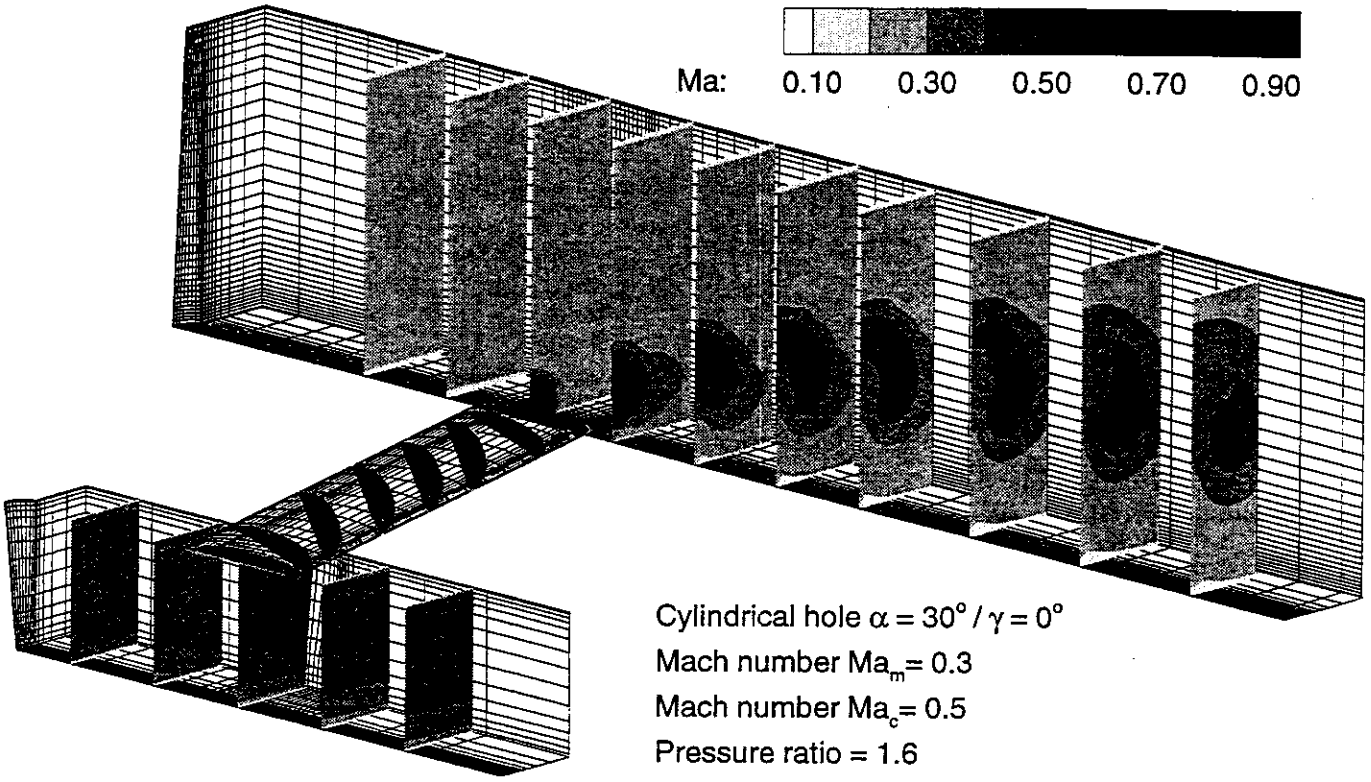

FIG. 11: Computed Mach contours on crossflow planes and inside the cylindrical film-cooling hole (α=30°, γ=0°)

perature were set at the entry of the primary and secondary channel, and static pressure was set at the exit of primary and secondary channel. The flow through the film-cooling hole was not taken from the experiment, but resulted from the calculated pressure distribution across the hole. The computed flow rates in the primary and secondary channel, as well as through the film-cooling hole, were very close to the measured flow rates demonstrating the capability of the code. The calculated blowing ratio showed a maximum deviation of 5% from the measured blowing ratio.

Figure 11 shows the computed Mach number contours. The dominating flowfield mechanisms are clearly evident in Figure 11 which include a strong acceleration of coolant fluid as it enters the cooling hole. In addition, the development of a pair of lateral vortices occur after the jet exits the cooling hole which entrain main flow into the wake of the jet.

Figure 12 shows a comparison of the streamwise and vertical mean velocity contours calculated using the CFD code and measured using the LDV system. The mass flow ejected through the hole was predicted to be about 5 % higher than the measured mass flow resulting in slightly higher predicted values of the streamwise and vertical velocity at the exit of the hole. Most of the jet is ejected from the downstream portion of the hole which was predicted correctly. The position of the maximum vertical velocity downstream of the hole, due to the main flow penetrating under the jet, is predicted too high, too far downstream, and too far away from the wall.

Generally, the simulations are in good agreement with the experiments. However, some discrepancies were found when comparing the mean velocities and turbulence quantities inside the hole and at the hole exit plane. In particular, the prediction for the highly three-dimensional flow inside the hole differ significantly from the measurements documented by Thole, Gritsch, Schulz, and Wittig (1996a). Since the computed solution was fully converged, these effects are believed to be either due to grid dependancy of the solution or, more likely, attributed to the k-ϵ turbulence model. The very complex flowfield inside the hole could not be predicted accurately due to the highly anisotropic turbulence field. These findings agree with the results reported by Leylek and Zerkle (1993). Therefore, future work will consider both possibilities, but emphasize evaluations of more suitable turbulence models.

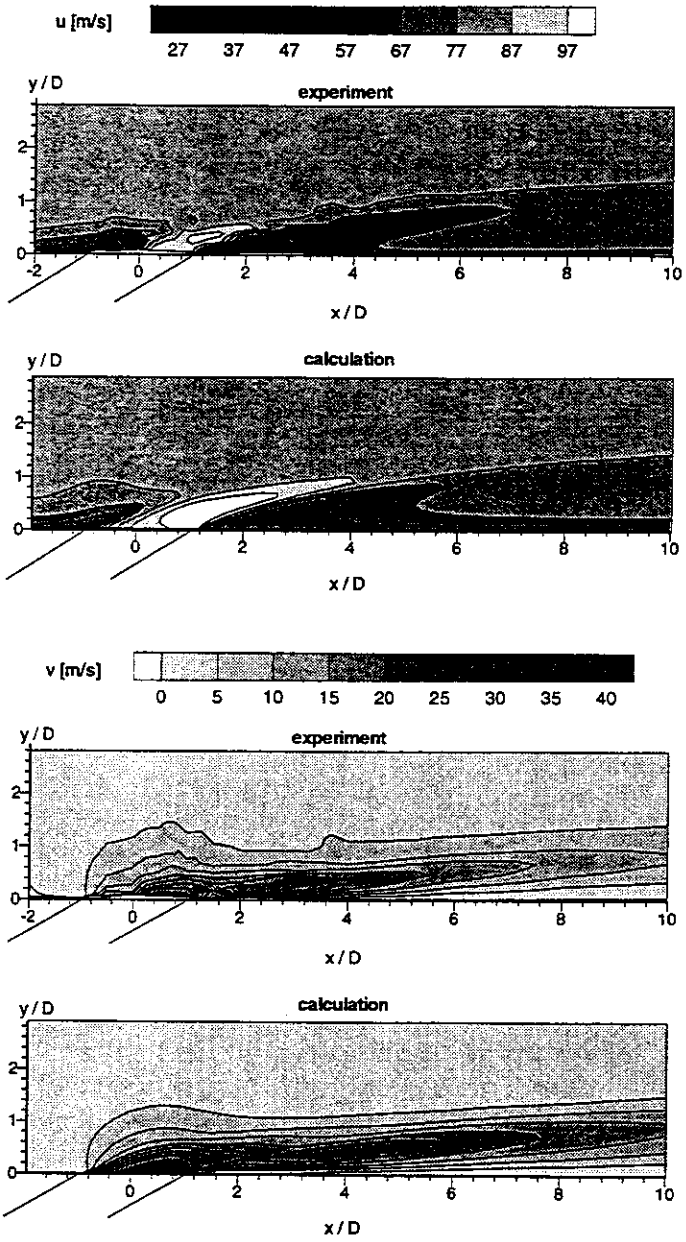

FIG. 12: Measured and predicted mean velocity contours on centerline plane of the primary channel (Ma_m=0.25, Ma_c=0.3, M=1, I=1) for the basecase cylindrical hole ejection (α=30°,γ=0°)

CONCLUSIONS

A new film-cooling test rig has been designed and built at the Institut für Thermische Strömungsmaschinen. The design constraints, construction, and features of the rig as well as its instrumentation and the measuring techniques applied are described in detail. A comprehensive summary of both present and future experimental and numerical programs were given. Examples of the measurements previously obtained have been presented. The results demonstrate the capability of the test rig to provide useful data for testing film-cooling configurations, particularly at transonic main flow conditions.

ACKNOWLEDGMENTS

This study was partly funded by the European Union through grant by the Brite Euram program "Investigation of the Aerodynamics and Cooling of Advanced Engine Turbine Componenents" under Contract AER2-CT92-0044. The authors wish to express their gratitude to the partners involved in the program and to R. Clifford from Rolls-Royce plc who played an active role in initiating and co-ordinating the work program.

REFERENCES

Benz, E. and S. Wittig (1992). Prediction of the Interaction of Coolant Ejection with the Main Stream at the Leading Edge of Turbine Blade : Attached Grid Application. In *Int. Sym. Heat Transfer in Turbomachinery*, Athens, Greece, August 24-28, 1992.

Benz, E., S. Wittig, A. Beeck, and L. Fottner (1993). Analysis of Cooling Jets near the Leading Edge of Turbine Blades . In *72nd Fluid Dynamics Panel Meeting and Symposium on "Computational and Experimental Assessment of Jets in Cross Flow"*, Winchester, U.K., April 19-22, 1993.

Colladay, R. and L. Russell (1976). Streakline Flow Visualization of Discrete Hole Film Cooling for Gas Turbine Applications . *ASME Journal of Heat Transfer*, Vol. 98, pp. 245–250.

Garg, V. and R. Gaugler (1995). Leading Edge Film Cooling Effects on Turbine Blade Heat Transfer . ASME Paper 95-GT-275.

Giebert, D., H.-J. Bauer, and S. Wittig (1996). A comparative Study of two low-Reynolds number k-ϵ turbulence models for recirculating flows with and without heat transfer. Accepted for publication at the 3rd International Symposium on Engineering Turbulence Modelling and Measurements, Crete, Greece, May 27-29, 1996.

Goldstein, R., E. Eckert, and F. Burggraf (1974). Effects of Hole Geometry and Density on Three–Dimensional Film Cooling. *Int. J. Heat Mass Transfer*, Vol. 17, pp. 595–607.

Goldstein, R., E. Eckert, V. Eriksen, and J. Ramsey (1970). Film Cooling Following Injection Through

Inclined Circular Tubes. *Israel Journal of Technology*, Vol. 8, pp. 145–154.

Haller, B. and J. Camus (1983). Aerodynamic Loss Penalty Produced by Film Cooling Transonic Turbine Blades. ASME Paper 83-GT-77.

Hay, N., S. Henshall, and A. Manning (1992). Discharge Coefficients of Holes Angled to the Flow Direction . ASME Paper 92-GT-192.

Hay, N. and D. Lampard (1995). The Discharge Coefficient of Flared Film Cooling Holes . ASME Paper 95-GT-15.

Hay, N., D. Lampard, and S. Benmansour (1983). Effect of Crossflows on the Discharge Coefficient on Film Cooling Holes . *ASME Journal of Engineering for Power*, Vol. 105, pp. 243–248.

Hay, N. and A. Spencer (1991). Discharge Coefficients of Cooling Holes with Radiused and Chamfered Inlets . ASME Paper 91-GT-269.

Honami, S., T. Shizawa, and A. Uchiyama (1992). Behaviors of the Laterally Injected Jet in the Film Cooling: Measurements of Surface Temperature and Velocity/Temperature Field within the Jet. ASME Paper 92-GT-180.

Jubran, B. and A. Brown (1985). Film Cooling From Two Rows of Holes Inclined in the Streamwise and Spanwise Direction. *ASME Journal of Engineering for Gas Turbines and Power*, Vol. 107, pp. 84–91.

Kurreck, M. and S. Wittig (1994). Numerical Simulation of Combustor Flows on Parallel Computers - Potential, Limitations and Practical Experience. ASME Paper 94-GT-404.

Leylek, J. and R. Zerkle (1993). Discrete-Jet Film Cooling: A Comparison of Computational Results with Experiments . ASME Paper 93-GT-207.

Liess, C. (1975). Experimental Investigation of Film Cooling With Ejection From a Row of Holes for the Application to Gas Turbine Blades. *ASME Journal of Engineering for Power*, Vol. 97, pp. 21–27.

Ligrani, P., J. Wigle, S. Ciriello, and S. Jackson (1994). Film-Cooling From Holes With Compound Angle Orientations: Part 1 – Results Downstream of Two Staggered Rows of Holes With 3d Spanwise Spacing . *ASME Journal of Heat Transfer*, Vol. 116, pp. 341–352.

Makki, Y. and G. Jakubowski (1986). An Experimental Study of Film Cooling from Diffused Trapezoidal Shaped Holes. AIAA Paper 86-1326.

Martiny, M., A. Schulz, and S. Wittig (1995). Full-Coverage Film Cooling Investigations: Adiabatic Wall Temperatures and Flow Visualization. ASME Paper 95-WA/GT-4.

Noll, B. (1992). Evaluation of a Bounded High-Resolution Scheme for Combustor Flow Computations . *AIAA Journal*, Vol. 30, pp. 64–69.

Noll, B. and S. Wittig (1991). Generalized Conjugate Gradient Method for the Efficient Solution of Three-Dimensional Fluid Flow Problems. *Numerical Heat Transfer, Part B*, Vol. 20, pp. 207–221.

Patankar, S. and D. Spalding (1972). A Calculation Procedure for Heat, Mass and Momentum Transfer in Three-Dimensional Parabolic Flows. *Int. J. Heat Mass Transfer*, Vol. 15, pp. 1787–1806.

Sathyamurthy, P. and S. Patankar (1990). Prediction of film cooling with lateral injection. In *Heat transfer in turbulent flow. 5. AIAA-ASME Thermophysics and Heat Transfer Conference (Seattle, Wash.)*.

Scherer, V., S. Wittig, K. Morad, and N. Mikhael (1991). Jets in a Crossflow: Effects of Hole Spacing to Diameter Ratio on the Spatial Distribution of Heat Transfer. ASME Paper 91-GT-356.

Schmidt, D., B. Sen, and D. Bogard (1994). Film Cooling with Compound Angle Holes: Adiabatic Effectiveness. ASME Paper 94-GT-312.

Sen, B., D. Schmidt, and D. Bogard (1994). Film Cooling with Compound Angle Holes: Heat Transfer. ASME Paper 94-GT-311.

Sinha, A., D. Bogard, and M. Crawford (1990). Film Cooling Effectiveness Downstream of a Single Row of Holes with Variable Density Ratio . ASME Paper 90-GT-43.

Thole, K., M. Gritsch, A. Schulz, and S. Wittig (1996a). Effect of Inlet Conditions for Jet-in-Crossflow as Applied to Film-Cooling . submitted to the ASME Journal of Fluids Engineering.

Thole, K., M. Gritsch, A. Schulz, and S. Wittig (1996b). Flowfield Measurements for Film-Cooling Holes with Expanded Exits. to be presented at the International Gas Turbine & Aeroengine Congress and Exhibition, Birmingham, UK, June 10-13, 1996.

Wittig, S., H.-J. Bauer, and B. Noll (1987). On the Application of Finite-Difference Techniques for the Computation of the Flow Field in Gas Turbine Combustors with Complex Geometries. In *Combustion and Fuels in Gas Turbine Engines*. AGARD-CP-422, Paper 28.